# Magnetic and electron transport properties of single-crystal UPtGe

R. Troć, J. Stępień-Damm, and C. Sułkowski
*W. Trzebiatowski Institute for Low Temperature and Structure Research, Polish Academy of Sciences, P.O. Box 1410, 50-950 Wrocław, Poland*

A. M. Strydom*
*Physics Department, Rand Afrikaans University, P.O. Box 524, Auckland Park 2006, Johannesburg, South Africa*
(Received 5 September 2003; revised manuscript received 21 November 2003; published 22 March 2004)

UPtGe orders below 50 K in a magnetic structure with the uranium $5f$-magnetic moments arranged in a cycloid in the $ac$ plane on a noncentrosymmetric orthorhombic crystal structure. The propagation vector $\boldsymbol{q}=(0.55,0,0)$ is directed along the $a$ axis. There is very little magnetocrystalline anisotropy within the $ac$ plane, compared to a large anisotropy between the two in-plane directions and the out-of-plane direction, as seen in various type of measurements. We present here results of measurements of single-crystalline magnetic susceptibility, electrical resistivity, magnetoresistivity, and thermoelectric power in order to investigate the consequences of the complex magnetic structure on the electronic behavior in UPtGe. As a result of a change in the Brillouin zone at $T_N$, a (pseudo)gap opens in the conduction electron band along the three principal directions. The appearance of magnetic zone boundaries due to the complex antiferromagnetic order in UPtGe is seen in the low-temperature variation of the thermoelectric power exhibiting pronounced maxima far below $T_N$ along the three main crystallographic directions.

DOI: 10.1103/PhysRevB.69.094422 PACS number(s): 75.20.Hr, 72.15.Gd, 75.40.Cx

## I. INTRODUCTION

The equiatomic ternary U$TM$ family of numerous uranium compounds ($T=d$-electron metal, $M=p$-electron metal) is exceptionally rich in physical properties.[1] There are four major crystal structure types among U$TM$ compounds that provide the basis for an extensive variation in the degree of $5f$-electron hybridization with ligand electrons which is, in turn, a deciding factor in the formation of stable magnetic moments in the solid state. Long-range magnetic ordering among the $5f$-electron moments, which usually takes place at several tens of K, as well as a temperature or field-induced variation in the magnetic order, is especially prevalent among U$TM$ compounds.

The systematics of the magnetic[2] and electrical properties[3] of a number of U$T$Ge germanides were initially investigated on polycrystalline samples. It is well known that in a series of ternary uranium isostructural compounds such as U$T$Ge, the presence of heavier transition elements, such as Ni, Pd, or Pt, generally stabilizes the narrow-band $5f$-electron moment formation as a precursor to magnetic ordering effects. With the exception of the Fe-,[4] Co-, and Ru-containing compounds, magnetic ordering was found[2] in all the germanides. Evidence was put forward for anomalous behavior in the character of the ordering that takes place in UPtGe. The inverse susceptibility $\chi^{-1}$ was measured on a powder sample and found to increase first continuously upon cooling through $T_N(=52\ \mathrm{K})$, but then it becomes nearly temperature independent below $\sim 25$ K. A similar behavior was observed on a single-crystal sample when $H\|a$.[5] On the other hand, the electrical resistivity $\rho(T)$ of UPtGe increases rapidly at $T_N$, and peaks near 20 K.[3] Neither of these distinct attributes were seen in the vicinity of the respective ordering temperatures for any of the other investigated equiatomic silicides or germanides.[2,3] The increase in $\rho(T)$ just below $T_N$ could be associated with a decrease in the effective number of charge carriers upon reformation of the Brillouin zone boundaries when the magnetic unit cell becomes different from the crystallographic unit cell. Kawamata *et al.*[6] found on their single-crystalline electrical measurements along the $c$ axis, an enhancement of the resistivity in UPtGe caused by the magnetic superzone effect, as was the case on the polycrystalline sample. Moreover, they found for all U$T$Ge ($T$ = Ni, Pd, Pt) a Kondo-like behavior between 100−300 K. From the initial exploratory measurements[5] of magnetic susceptibility made on single-crystal UPtGe up to 200 K, a small in-plane magnetocrystalline anisotropy was contrasted against a comparitively large out-of-plane anisotropy. The susceptibility data of Kawamata *et al.*[5] for the field along the orthorhombic $b$ axis ($\chi_b$) revealed no distinct anomaly in the vicinity of $T_N$, suggesting that $\chi_b$ does not reflect any major component of the ordered magnetic moment in this direction.

The results of powder neutron diffraction measurements on UPtGe led Szytuła *et al.*[7] to favor the TiNiSn-type structure (*Pnma*) instead of the previously adopted $CeCu_2$ type (*Imma*).[2,5] The TiNiSi-type structure represents positional ordering among the Pt and the Ge atoms in UPtGe, and may be described by an interchange of the $a$ and $b$ axes with respect to the $CeCu_2$-type structure. Furthermore, based on this crystal structure, Robinson *et al.*[8] (also using polycrystalline samples) and Kawamata *et al.*[9] (single-crystal sample) put forward an interesting model of incommensurate $5f$-electron magnetic moment ordering in UPtGe. According to this model, the moments were determined to form a cycloid structure that is unique among actinide systems. The question of the crystal structure in UPtGe that could form the basis for such an exceptional arrangement of magnetic moments has recently been the subject of an in-depth neutron and resonant magnetic x-ray study reported by Mannix *et al.*[10] According to these authors the prefered structure is

 

TABLE I. Crystal data structure and refinement parameters for UPtGe.

| Structure parameter | Room-temperature data | Low-temperature data |
|---|---|---|
| Empirical formula | Ge Pt U | |
| Formula weight | 505.71 | |
| Temperature | 293(2) K | 15(1) K |
| Crystal system, space group | orthorhombic, $Imm2$ | |
| Unit cell dimensions | $a=4.333(1)$ Å | $a=4.320(1)$ Å |
| | $b=7.199(1)$ Å | $b=7.161(1)$ Å |
| | $c=7.528(2)$ Å | $c=7.507(2)$ Å |
| Volume | 234.82(9) Å$^3$ | 232.23(9) Å$^3$ |
| Theta range for data collection | 3.92° to 36.95° | 3.93° to 28.85° |
| Reflections collected/unique | 1683/506 [$R$(int)=0.0894] | 661/308 [$R$(int)=0.0747] |
| Data/restraints/parameters | 506/1/22 | 308/1/22 |
| Goodness-of-fit on $F^2$ | 1.157 | 1.198 |
| Final $R$ indices [$I>2\sigma(I)$] | $R_1=0.0399$, $wR_2=0.1095$ | $R_1=0.0482$, $wR_2=0.1219$ |
| $R$ indices (all data) | $R_1=0.0409$, $wR_2=0.1100$ | $R_1=0.0489$, $wR_2=0.1226$ |
| Absolute structure parameter | 0.02(5) | −0.13(8) |
| Extinction coefficient | 0.0180(13) | 0.0086(10) |

the orthorhombic EuAuGe-type structure ($Imm2$) instead, which is in contrast to the $CeCu_2$ and TiNiSi types, a noncentrosymmetric structure having again the same axial nomenclature as that of the $CeCu_2$-type structure (i.e., $a$ and $b$ axes interchanged with respect to TiNiSi). In this structure, in contrast to the other two types, there are two crystallographically different sites occupied by the uranium atoms, one platinum site, and one germanium site. Further details of both the crystal and magnetic structure of UPtGe can be found in the discussion further below.

Some preliminary data on a UPtGe single crystal were presented in a conference article.[11] The purpose of this study is to compliment the existing crystallographic and magnetic structural investigations on UPtGe with data on physical properties including magnetization, electrical resistivity, magnetoresistivity, and thermoelectric power. We are placing emphasis on the anisotropic behavior and the response to the magnetic field applied along the three main crystal axes $a$, $b$, and $c$, with respect to the EuAuGe-type structure.

## II. EXPERIMENTAL

A single crystal of UPtGe was prepared from a stoichiometric melt using the Czochralski method, with starting elements (of purity in weight percent) U (99.98), Pt (99.99), and Ge (99.999). No further heat treatment was given to the as-grown single-crystal button. We used electron microprobe analyses to verify the good quality of the obtained single crystals. The sample was cut by an abrasive wire into pieces with appropriate geometries for the various measurements. A small part of the single crystal was powdered by crushing to aid crystal-structure refinement by x-ray diffraction. Single-crystal x-ray diffraction was performed at room temperature and 15 K on an Xcalibur 2 four-circle diffractometer equipped with a CCD camera and a Heli-jet cryosystem using a graphite-monochromatized Mo-$K\alpha$ radiation. The intensities of reflections were corrected for Lorentz and polarization effects. The crystal data were refined by the full least squares method using the SHELX-97 program.[12]

Magnetization and susceptibility measurements were performed using a commercial superconduction quantum interference device (SQUID) magnetometer in temperatures from 400 K down to 1.8 K and in fields up to 5 T, with the sample oriented along the main axes using the x-ray method. The electronic transport was measured using a steady-current, four-point method with spot-welded wire contacts on bar-shaped specimens measuring $1\times1\times6$ mm$^3$, in temperatures between 290 and 1.4 K, and in transverse magnetic fields ($i\perp B$) up to $B=\mu_0H=8$ T. The thermoelectric power was measured using a Keithley type 220 nanovoltmeter to sense the voltage drop over a temperature gradient of $\approx5$ K sustained across the two ends of a bar-shaped specimen similar to that used for resistivity measurements.

## III. RESULTS AND DISCUSSION

### A. Crystal and magnetic structure

In this work we have performed single-crystal x-ray refinement on data collected at room temperature and at 15 K. Results of the structural refinement are given in Tables I and II. Apart from ascertaining the good single-crystalline quality of our samples, the x-ray diffraction data have fully confirmed the results of Hoffmann *et al.*,[13] who reinvestigated the EuAuGe type structure (space group $Imm2$) of UPtGe and established the positional ordering of the Pt and Ge atoms within this structure.

The crystal structure was refined with anisotropic atomic displacement parameters for all atoms. Thus, these parameters were used to present in Fig. 1 the projections of the structure along the $a$ (left-hand panel) and $b$ (right-hand panel) axes. The U1 and U2 atoms are both coordinated by two puckered $Pt_3Ge_3$ hexagons located above and below the central atom, but with distinctly different respective bond lengths. Correspondingly, these atoms have either the closer

TABLE II. Atomic coordinates and anisotropic and equivalent isotropic displacement parameters ($10^3$ Å$^2$) for UPtGe at the respective measurement temperatures of 293 and 15 K.

| Atom | U1 | | U2 | | Pt | | Ge | |
|---|---|---|---|---|---|---|---|---|
| Site | 2*a* | | 2*b* | | 4*d* | | 4*d* | |
| *T* (K) | 293 | 15 | 293 | 15 | 293 | 15 | 293 | 15 |
| *x* | 0 | 0 | 0 | 0 | 0 | 0 | 0 | 0 |
| *y* | 0 | 0 | 1/2 | 1/2 | 0.2080(2) | 0.2068(3) | 0.2796(5) | 0.2811(8) |
| *z* | 0.4719(1) | 0.4707(3) | 0.5372(1) | 0.5383(3) | 0.8343(1) | 0.8342(2) | 0.1639(3) | 0.1638(6) |
| $U_{11}$ | 12(1) | 4(1) | 8(1) | 4(1) | 8(1) | 3(1) | 8(1) | 1(1) |
| $U_{22}$ | 11(1) | 0(1) | 10(1) | 0(1) | 13(1) | 0(1) | 17(1) | 0(2) |
| $U_{33}$ | 7(1) | 5(1) | 9(1) | 3(1) | 7(1) | 5(1) | 7(1) | 2(3) |
| $U_{23}$ | 0 | 0 | 0 | 0 | 0(1) | 0(1) | −1(1) | 1(2) |
| $U$(eq) | 10(1) | 3(1) | 9(1) | 2(1) | 9(1) | 3(1) | 11(1) | 3(1) |

germanium (U1 and Ge) or platinum (U2 and Pt) nearest-neighbor distances which in turn are significantly longer than the sums of the metallic atomic radii (U+Ge) and (U+Pt), respectively. This feature is quite the opposite to the three-dimensional $Pt_3Ge_3$ hexagons, having Pt-Ge contacts in good agreement with the sum of Pauling's single-bond radii.[13] These structural differences are well reflected in the magnetic behavior of UPtGe leading in consequence to two different values of the ordered moment for the U1 and U2 sites.[10] The refinement of the crystal structure of UPtGe at low temperature has not revealed any significant difference with that at room temperature, except the change in the unit-cell volume by about 1.1%, emphasizing the fact that the formation of the cycloidal magnetic structure does not cause any distortion of the lattice. This result is, for example, in contrast with the situation found in hexagonal UPdSn (Ref. 14) where a distortion was observed first to the orthorhombic unit cell at $T_N = 40$ K, and then to a monoclinic unit cell at the temperature of 25 K where another magnetic transition occurs.

In order to describe the cycloid magnetic structure we have marked by arrows in Fig. 1 the arrangement of the magnetic moments in the uranium lattice sites of the *ac* plane that form a structure close to a simple haxagon with an additional uranium atom at its center. We took into account also the fact that the phase angle $\phi$ between the two cycloids, corresponding to the U1 and U2 atoms, is close to zero. The propagation vector $\boldsymbol{q}$ of the magnetic structure is along the *a* direction with the value of [0.55(1), 0, 0] (Ref. 10) in accordance with those given by earlier papers.[7–9] Moreover, the ellipticity $\epsilon$ defined as the ratio $\mu[100]/\mu[001]$ for both moments is close to the average value of 1.24,[10] which can reflect the fact that $\chi_a > \chi_c$ at 4.2 K. This, however, is reversed at $T_N$. The nature of the unique magnetic structure has been studied with density functional theory by Sandratskii and Lander.[15] They have shown that the formation of the cycloid results from coexistence of an accidentally small in-plane magnetic anisotropy and frustrated exchange interactions. As seen in Fig. 1, the arrangement of atoms in the corners of triangles within a given hexagon leads immediately to the geometrical frustration among the moments in the case of existence of the antiferromagnetic type interaction between them. The calculation results reflect also an important influence of the position of the Pt and Ge atoms on the magnetic behavior of UPtGe.

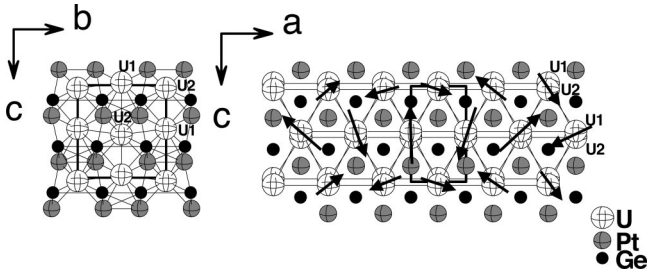


FIG. 1. Schematic display of the crystal structure of UPtGe. In the left-hand panel, the projection onto the *bc* plane of a unit cell of the orthorhombic EuAuGe-type structure is shown (*a* is directed perpendicularly out of the plane) to illustrate the two different actinide sites, U1 located at $(0,0,z)$ and U2 at $(0,\frac{1}{2},z)$. The right-hand panel (*b* is directed perpendicularly into the plane) shows the projection onto the *ac* plane with the cycloidal arrangement of the magnetic moments in the ordered state indicated by arrows. For the sake of simplicity we have shown the cycloid in only one (upper) *ac* plane containing both the U1 (longer arrows) and U2 (shorter arrows) moments.

### B. Magnetic properties

Figures 2(a) and 2(b) show the temperature dependence of respectively the magnetic susceptibility $\chi_i(T)$ and the reverse magnetic susceptibility $\chi_i^{-1}(T)$ for UPtGe, with a measuring field equal to $B = 0.5$ T along the three respective orthorhombic crystal axes $(i = a,b,c)$. For comparison we also show the polycrystalline data measured on a fixed, solid sample (diamond symbols). The anomaly in $\chi$ at $T = 50$ K (marked by an arrow) that is evident in all the data sets, is taken as the onset of the antiferromagnetic state. The single-crystal data are in agreement with that of Kawamata *et al.*,[5] except that in our susceptibility data there is a more distinct anomaly seen in $\chi_b(T)$ at $T_N$ for $B \| b$, apart from the sharp features at this temperature for fields applied along the other two directions, i.e., for $\chi_a$ and $\chi_c$ at $T_N$, where $\chi_c > \chi_a$. The thin solid lines superimposed upon the respective data sets in Fig. 2(b) represent the results of least-squares fits of the modified Curie-Weiss (MCW) law

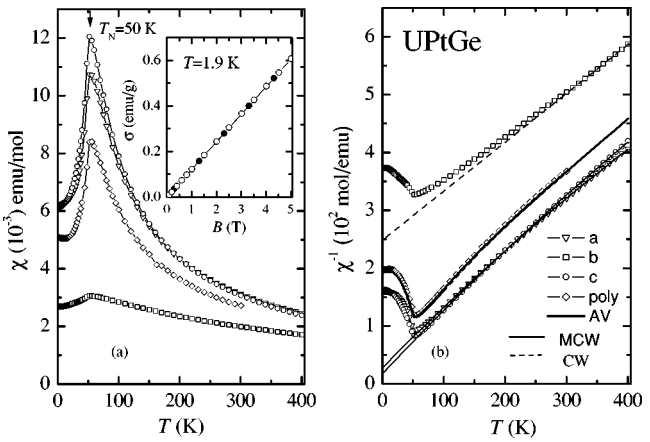


FIG. 2. The temperature dependence of (a) the magnetic susceptibility $\chi(T)$, and (b) the inverse susceptibility $\chi^{-1}(T)$, for single-crystal UPtGe along the three main directions *a*, *b*, and *c*. The $T=1.9$ K isothermal magnetization (*c* direction) is shown in the inset of (a). The solid lines superimposed onto the data in (a) are guides to the eye. In (b) the solid lines indicate the results of least-squares fits of a modified Curie-Weiss law for $B\|a,c$, while the dashed line represents a Curie-Weiss law for $B\|b$. Furthermore, the calculated average susceptibility is indicated by a solid line on the polycrystalline data points (see text).

$$\chi(T)=\chi_0+\frac{n\mu_B\mu_{\rm eff}^2}{3k_B(T-\theta_P)}. \tag{1}$$

The modification is due to the downward curvature in $\chi^{-1}(T)$ and is achieved through addition of the temperature-independent term $\chi_0$. In Eq. (1), $\theta_P$ is the paramagnetic Curie temperature, $\mu_{\rm eff}$ is the effective paramagnetic moment, and *n* is the molar concentration of magnetic moments. For the magnetic field along the *a* and *c* directions this law adequately describes the $T>T_N$ data, with parameters as listed in Table III. In contrast to these, the $\chi_b^{-1}(T)$ dependence deviates below 200 K in the upward direction and above this temperature the susceptibility obeys an ordinary Curie-Weiss law (dashed line). In polycrystalline samples a strong magnetic anisotropy can be expected to produce a low-temperature curvature in $\chi_{\rm poly}^{-1}(T)$ leading to rather unreliable magnetic parameters. Nevertheless, we have found a good agreement of the observed $\chi_{\rm poly}^{-1}(T)$ with the calculated average reciprocal susceptibility $\chi_{\rm av}^{-1}(T)$ (thick line), where

$$\chi_{\rm av}=\frac{\chi_a+\chi_b+\chi_c}{3}. \tag{2}$$

We note that the calculated effective moment value obtained for the polycrystalline sample compares rather well with those of the two magnetically easy directions. As seen from Fig. 2, along the *a* and *c* directions, the measured $\chi_a(T)$ and $\chi_c(T)$ concur a very small in-plane magnetocrystalline anisotropy, compared to the out-of-plane susceptibility $\chi_b(T)$. The magnetic anisotropy in UPtGe is evident from several aspects: in the paramagnetic region the *b*-axis data project a much larger negative value of $\theta_P$. In the ordered region the *c*-axis susceptibility exceeds that of the *a*-axis susceptibility by about 10% [see the values of $\chi(T=T_N)$ in Table III], while the *b*-axis susceptibility measured at the same temperature amounts to only 25% of the *c*-axis value at $T_N$.

The weak temperature dependence of the susceptibility along the hard magnetization direction is usually governed by the single-ion anisotropy in the ground state for which the real wave functions are not now accessible. Among the three directions, the large moment value of $\mu_{\rm eff}=3.24\ \mu_B$/U yielded by the *b*-axis data is thus connected with a large contribution of a temperature-independent Van Vleck part in the overall susceptibility caused by the crystal electric field interaction on the anisotropic ground state. When seen together with the much larger $|\theta_p|$ value for the *b* direction, this gives a picture of substantially weakened correlations between the $5f$-electron moments between $ac$-moment planes in UPtGe.

As indicated in Fig. 2, the magnetic anisotropy is distinctly an easy-plane type. The paramagnetic Curie temperatures $\theta_p^i$ $(i=a,b,c)$ can be used to express qualitatively the magnitude of the magnetic anisotropy. While for the $ac$ plane $|\theta_p^a-\theta_p^c|=8$ K, the anisotropy in the $ab$ or $cb$ planes is much stronger and taking the above criterion it amounts to more than 300 K. The effective magnetic moments $\mu_{\rm eff}^a \approx \mu_{\rm eff}^c=2.66(1)\ \mu_B$. This value corresponds to the ground crystal-field state being either doublet or pseudo doublet for the $5f^3$ $(U^{3+})$ or $5f^2$ $(U^{4+})$ electron configuration respectively, in accordance with the $R\ln 2$ value of the magnetic entropy at $T_N$ reported in Ref. 16. It therefore indicates the localized character of the electrons in this compound, reflected also in the low value,[16] 25 mJ/($K^2$ mol), of the coefficient of electronic heat capacity.

A graph of the *c*-axis magnetization $\sigma(B)$ of UPtGe is shown in the inset of Fig. 2. We could not detect any hysteresis between the increasing and decreasing field data. The magnetization proceeds linearly with field, from the origin right up to 5 T, providing a good agreement of the $\sigma/H$ ratio at 4.2 K with $\chi_c$ at this temperature. Also the $\sigma/H$ slopes of the corresponding magnetization straight lines taken at 4.2 K

TABLE III. Least-squares fit parameter values for the magnetic properties of UPtGe (see Fig. 2).

| Sample alignment | $\theta_P$ (K) | $\mu_{\rm eff}$ ($\mu_B$) | $\chi_0$ ($10^{-4}$) emu/(mol U) | $\chi(T=T_N)$ ($10^{-3}$) emu/(mol U) |
|---|---|---|---|---|
| *a* | −22.8(1) | 2.66(1) | 3.5(1) | 10.7 (54 K) |
| *b* | −350(1) | 3.24(2) | 0 | 3.1 (52 K) |
| *c* | −15.1(1) | 2.67(3) | 2.9(1) | 12 (55 K) |
| polycrystal | −24.0(2) | 2.31(2) | 6.4(1) | 8.4 (56 K) |

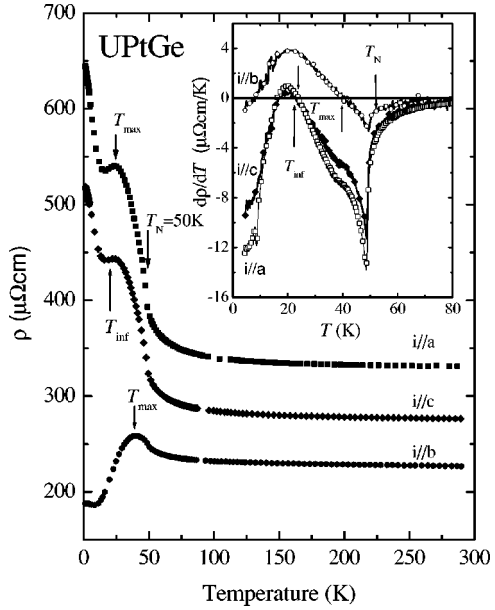


FIG. 3. The temperature dependence of the electrical resistivity $\rho(T)$ (main figure) and its temperature-derivative (inset) for single-crystal UPtGe along the three principal directions *a*, *b*, and *c*. The distinct features, as explained in the text, are indicated by arrows, viz. the Néel transition point $T_N$, the maximum $T_{\max}$ within the magnetic ordered region which is especially evident for current along the *b* direction, and an inflection point $T_{\inf}$ seen for $i\|a$ and $i\|c$ as a result of a continued increase in $\rho$ towards low temperatures for these two directions. For the *b* direction, the same $T_{\inf}$ corresponds instead to a continued *decrease* in $\rho$ towards low temperature.

in high magnetic fields[17] clearly indicate that $\chi_a > \chi_c \gg \chi_b$. In fact, in an applied field along the main axes up to 30.5 T an abrupt metamagnetic transition was observed for $B\|c$ and $B\|a$, without any sign of a similar effect for $B\|b$.[17] This high critical field indicates that the cycloid magnetic structure is fairly stable against an applied field. Moreover, the magnetization value obtained at 30.5 T for $B\|c$, being about 0.6 $\mu_B$, indicates the possible existence of another transition at higher applied fields, to reach the value of $1.0-1.1$ $\mu_B$, reported in neutron diffraction measurements.[7–9] A metamagnetic transition near 25 T was also reported by Buschow *et al.*[18] on a polycrystalline sample.

### C. Transport properties

#### *1. Electrical resistivity*

Figure 3 shows the zero-field resistivity data $\rho_i(T,B=0)$ for UPtGe. The semilogarithmic $\rho_i(T)$ graph has already been shown in previous work.[11] The measured resistivity values for the three directions *a*, *b*, and *c* at $T=290$ K amount to 329, 225, and 274 $\mu\Omega$ cm, respectively. The gradual increase in $\rho_i$ as the temperature is decreased from room temperature down to $T_N$ may be ascribed to the weak incoherent scattering mechanism of the single-ion Kondo effect that involves conduction electrons and the magnetic moments of nearly localized $5f$ electrons. A Kondo-like anomaly was also observed in single-crystalline measurements of UNiGe and UPdGe.[6] Apart from the observed variation in the absolute values in resistivity, there is seen only small anisotropy[11] in $\rho_i$ in the paramagnetic region as far as the temperature evolution is concerned. The magnetic ordering (marked by an arrow in Fig. 3) occurs with a sharp increase in $\rho$ for all three directions. We allocate $T_N$ to the point of the maximum rate of change of $\rho$ with temperature. As demonstrated in the inset to this figure, where the derivative $d\rho(T)/dT$ is plotted against temperature, for all three axes the sharp minimum at $T_N$ is well manifested with values in accordance with the magnetic data.

It can also be seen from the main graph of Fig. 3 that the resistivity reaches a local maximum for all three directions; deep within the ordered region, i.e., at $T_{\max}=22$ K for both $i\|a$ and $i\|c$, and at 41 K for $i\|b$. The occurrence of such a maximum in the resistivity is a consequence of Brillouin zone boundary reformation processes, such as the possible opening of a small gap in a part of the Fermi surface and hence a reduction in the effective number of charge carriers arising from the formation of an antiferromagnetic structure having a unit cell different from the chemical lattice. As was indicated above, the value of $T_{\max}$ differs by nearly 20 K between measurements of $\rho$ perpendicular to the moments ($i\|b$) and those parallel to the moment plane ($i\|a$ or $i\|c$).

Clearly, the resistivity becomes highly anisotropic in the ordered region below the local maximum, in the sense that *b* is the only axis along which the resistivity is found to decrease (by about 30%) towards near saturation as $T\to 0$. On the other hand, for the near-identical behavior of the $i\|a$ and $i\|c$ curves, i.e., for the current within the $ac$ plane where the moments are arranged in a cycloid, $\rho$ first reaches a local maximum and then continues to increase as $T\to 0$. This low-temperature limiting behavior for the in-plane resistivities could be fitted up to about 4 K to a phenomenological power law of the form $\rho(T)=\rho_0(1-AT^{3/2})$, as indicated by the solid lines superimposed onto the respective data sets in Fig. 4. We interpret the anisotropy seen in the electrical behavior on the basis of the way in which the moments are arranged in the ordered region. The cycloid is incommensurate with the crystal lattice and therefore precludes any periodic scattering potential from being formed in either the *a* or *c* direction. The low-temperature saturation for ($i\|a$) or ($i\|c$) is then due to the progressive freezing out of magnetic disorder scattering with decreasing temperature. On the contrary, the current parallel to *b* has on its way slightly buckled chains of uranium atoms running parallel to *b* (see Fig. 1) that effectively presents a near-periodic situation and so after going through a maximum, $\rho$ decreases accordingly to some constant value at $T=0$ K. The onset of saturation in the resistivity at low temperatures, irrespective of the current direction, is in agreement with the low-temperature demagnetization that occurs for all three directions also, as is seen in the susceptibility data (Fig. 2).

The magnetocrystalline anisotropy in UPtGe is further exemplified in Fig. 5 by measurements of the resistivity in a magnetic field up to 8 T. The difference in the isothermal transverse field dependence of magnetoresistivity (MR), defined as $\Delta\rho/\rho=[\rho(T,B)-\rho(T,0)]/\rho(T,0)$, taken for all

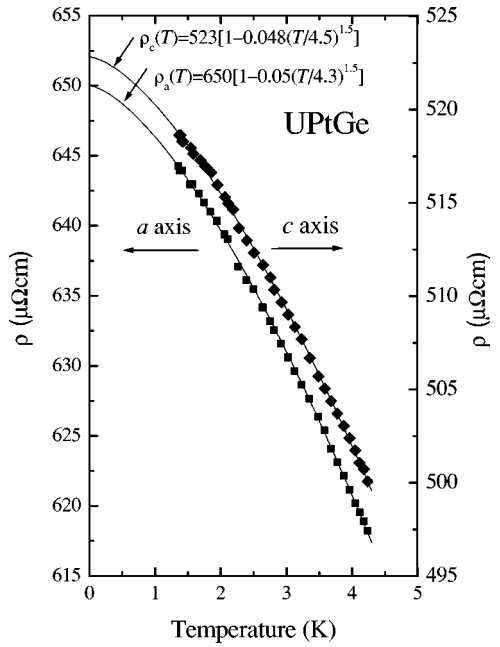


FIG. 4. The low-temperature resistivity of UPtGe for the *a* and *c* directions. The solid lines indicate the adherence of both data sets to a power law of the form $\rho(T)=\rho_0(1-AT^{1.5})$.

three directions $i\|a$, $i\|b$, and $i\|c$ is presented in Fig. 5(a). The situation for $i\|c$ is nearly identical to that of $i\|a$. For current in these directions and with the field perpendicular to these directions, it is seen that the MR is small and negative (MR $\simeq -0.3\%$ being the maximum value at 8 T). At low temperatures it behaves as $B^n$, with $n<2$ (see caption of Fig. 5). Nevertheless, the *negative* MR can be associated with the complex interaction with the field of the cycloidally arranged uranium moments. In contrast to this, for the compound UNiGe which has the TiNiSi-type crystal structure and with a commensurate magnetic structure with $\boldsymbol{q}=(0,1/2,1/2)$, a small, positive longitudinal MR was observed[19] just prior to the transition to a giant negative MR in fields generating metamagnetic transitions. The MR values obtained for UPtGe at 8 T by the field variation (large filled circles) closely follow the temperature variation of MR taken at a fixed 8 T field, the data of which are presented in Fig. 5(b). This indicates a high accuracy of the MR measurements, even if one is dealing with such small changes in MR. The small magnitudes of MR are in agreement with the local character of the magnetism in UPtGe and indicate the large stability of the cycloid structure. As high field magnetization studies demonstrated,[17] one can expect in the case of UPtGe a huge change in MR in fields as high as 30 T, where the metamagnetic transitions in UPtGe take place. This situation is somewhat different in respect to UNiGe,[19] where a giant MR (about 58%) could be observed already at 10 T, which is the critical field along the *c* axis. This huge MR was mainly interpreted as a suppression of the antiferromagnetic superzone by the field-induced ferromagnetic alignment.

Figure 5(b) also demonstrates for $i\|a$, $i\|b$, and $i\|c$ measured in $8T$, a sharp negative minimum at $T_N$ in the temperature dependences of MR, $\Delta\rho/\rho=f(T)$. Furthermore, the MR goes through a maximum near 20 K for $i\|a$ and $i\|c$, on

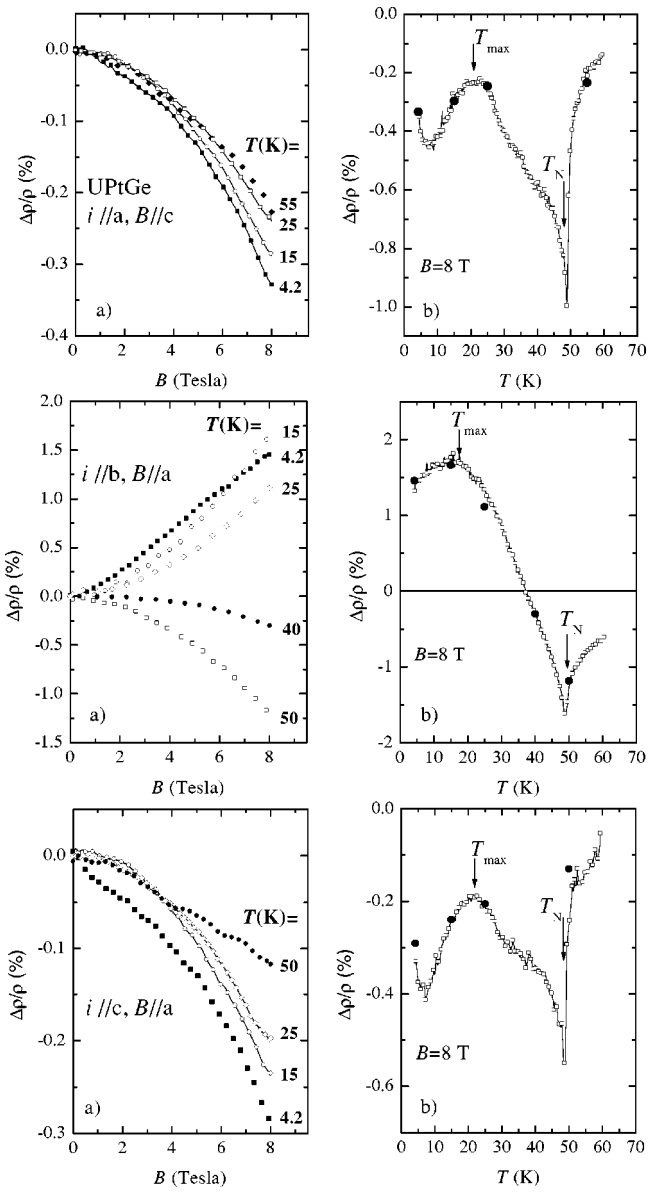


FIG. 5. The magnetoresistivity (MR) $\Delta\rho/\rho$ of UPtGe vs field (left-hand panels) and vs temperature for the fixed field of 8 T (right-hand panels) for the three principal crystal directions *a*, *b*, and *c*. On the right-hand panels the Néel point ($T_N$) and the peak positions ($T_{\max}$) are indicated by arrows. The large filled circles on the right-hand panels show the corresponding points obtained from the isothermal magnetoresistivity measurements. The low-temperature $\Delta\rho/\rho$ vs *B* curves for the *a* and *c* directions follow a $B^n$ dependence with $n=1.75$ and 1.5, respectively (not shown).

the one hand, and for $i\|b$ near 15 K on the other. These maxima are probably connected with the common inflection points of $T_{\inf}$ (see Fig. 3). The event of magnetic ordering causes MR ($B=8$ T) for $i\|b$ to pass through zero at 38 K, very near to the temperature of $\rho_{\max}(T,B=0)$, and consequently turning positive towards low temperatures. Similar to the situation for the hard direction is the behavior of MR for the polycrystalline sample (not shown), thus resembling the abovementioned similarity in the shapes of $\rho_{\text{poly}}(T)$ and $\rho_b(T)$. A positive MR, as is seen for $i\|b$, is typical of the

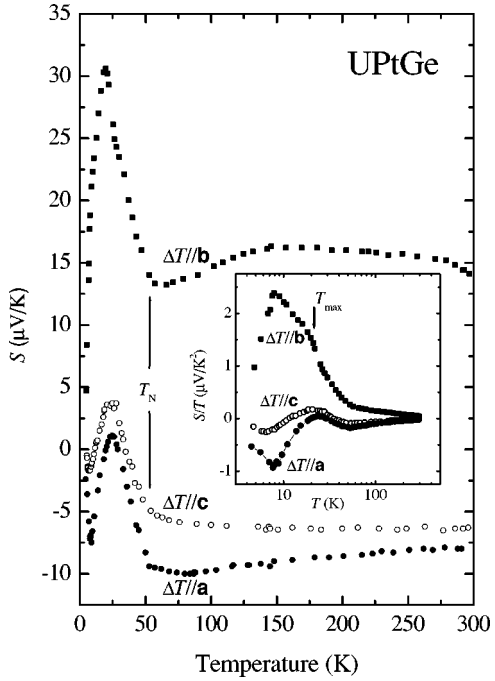


FIG. 6. The thermoelectric power $S(T)$ vs temperature for the three crystallographic directions *a*, *b*, and *c* of UPtGe. $S_i(T)$ sharply increases near $T_N$ (see arrow in the main figure) before reaching a common maximum near 20 K for all three directions.

effect of an applied magnetic field on the coherence, an effect which dominates the behavior of the zero-field resistivity along the *b* direction in the ground state. It is interesting to note that *all* the derivative curves show close to the temperature of about 20 K a maximum pointing to the existence of inflection points (marked as $T_{\mathrm{inf}}$) in spite of increasing (*a*, *c* axes) or decreasing (*b* axis) resistivities (see Fig. 3).

The Hall coefficient ($R_H$) was measured in the configuration $i \| a$ and $B \| c$ (not shown). In the paramagnetic region $R_H$ increases monotonically upon cooling down to $T_N$ and then decreases in accordance with the curve for the *c* axis susceptibility $\chi_c(T)$. Therefore it can be described using the expression

$$R_H = R_0 + 4\pi\chi_c(T) \cdot R_S, \tag{3}$$

where $R_0$ is the ordinary Hall coefficient and $R_S$ is the anomalous Hall coefficient. A good fit of the above equation to the experimental data is obtained almost from $T \geqslant T_N$. The obtained least-squares fit parameters amount to $R_0 = -3.1 \times 10^{-9}$ m$^3$/C and $R_S = 8.8 \times 10^{-6}$ m$^3$/C. Assuming a single-band description we obtain a carrier number $n = 0.2 \times 10^{21}$ electrons/cm$^{-3}$ or equivalently 0.01 electrons/f.u. The value of $R_S$, which is three orders of magnitude greater than $R_0$, emphasizes the fact that the $5f$-electron moments are localized centers of scattering with respect to the conduction electrons.

#### *2. Thermoelectric power*

Figure 6 illustrates the behavior of the thermoelectric power (TEP) $S_i(T)$ for the three crystallographic directions ($a$, $b$, $c$) in single-crystalline UPtGe. In the paramagnetic region the data for $S_a$ and $S_c$, i.e., when the temperature gradient $\Delta T$ is applied along the *a* and *c* directions, are either almost temperature independent ($S_c$) or weakly temperature dependent ($S_a$) and showing only a small difference in their room-temperature values ($-8$ and $-6.5$ $\mu$ V/K, respectively). On the contrary, the *b*-direction thermoelectric power ($S_b$) yields a fairly large, positive value of $+14$ $\mu$V/K at room temperature and goes through a broad maximum near 140 K in the paramagnetic region. Such a maximum in $S(T)$ has been identified as one of the prototype behaviors of narrow-band effects in cerium[20] and uranium compounds,[21] very often connected with the combined Kondo and crystal-electric field effects where usually an overall crystal-field splitting energy $\Delta$ is equal to $3T_{\mathrm{max}}$.[22] Also of interest is the fact that a distinct minimum is achieved at 60 K in $S_b$, prior to a steep increase upon further lowering of temperature which is seen in $S(T)$ for all three crystallographic directions (see arrows in Fig. 6) and in $S/T$ vs $\ln T$ (see the inset of Fig. 6), and which is associated with the magnetic ordering process at $T_N (= 50$ K). A precursor effect like this in the temperature dependence of the TEP is associated with the development of moment coupling just prior to long-range antiferromagnetic ordering.[23] Near 23 K the thermopower passes through a positive maximum and reaches values amounting to $S_a = +1.1$ $\mu$V K$^{-1}$ and $S_c = +3.7$ $\mu$V K$^{-1}$ for the two respective in-plane directions. On further cooling, $S(T)$ for both these directions tends to go through a negative minimum before $T = 0$ K is reached. The inset in Fig. 6 indicates a convergent behavior of $S_i(T)$ towards the lowest temperatures.

In general, $S_{a,c}(T)$ has features characteristic of a number of antiferromagnetic Kondo compounds.[24] A systematically enhanced thermoelectric power for intermetallic uranium compounds may be understood in terms of the Mott[25] relation between $S$ and an increased electronic density of states at the Fermi level, which is commonly found in many cerium[20,24] and uranium intermetallic compounds.[24,26] The $S(T)$ maximum observed at around 20 K corresponds roughly to $T_{\mathrm{inf}}$ defined from the $\rho_i(T)$ curves (see Fig. 3 and the inset). The appearance of maxima in $S_i(T)$ for all three directions well inside the ordered region compares favorably for example with the behavior of $S(T)$ found in single-crystalline UNiAl,[27] a hexagonal compound that orders antiferromagnetically at 19.3 K in a complex, anisotropic magnetic structure.[28] The moments are also arranged at the corners of triangles in the basal plane, similar to those described for UPtGe.

Moreover, as is the case of $S_b(T)$ in UPtGe, the TEP of UNiAl along the hexagonal *c* axis is positive in the whole temperature range, and peaks at a temperature of 10 K which is also well within the ordered region.[27] Thus, this behavior is fully reminiscent of that of $S_{a,c}(T)$ in UPtGe. Hence the interpretation of the TEP results in these two uranium ternaries should be convergent. We can also assume after Ref. 27 that the phonon or magnon drag contribution to the total TEP plays a rather minor role in $S_i(T)$. Taking into account only the electron diffusion $S_d(T)$, one may consider a more reli-

able two-band model[29] in which the conduction electrons with density of states (DOS) $N_s$ are scattered by $5f$ electrons with a relaxation rate $\tau_f^{-1}$ and DOS $N_f$. We obtain

$$S_d = \frac{\pi^2 k_B^2}{|3e|} T\left(\frac{\partial \ln N_s}{\partial E} - \frac{\partial \ln N_f}{\partial E}\right)_{E=E_F}. \quad (4)$$

Thus, the temperature dependence of the second term leads to a nonlinearity of $S$ vs $T$ and may yield a large value of $S_d$, which is a rather common phenomenon in uranium intermetallics.[24,26] As a consequence of Brillouin effects in the ordered state, the maxima in $S_i(T)$ are seen in the three principal directions of UPtGe, which arise due to the opening of a gap (or pseudogap) at the Fermi energy ($E_F$) in the DOS of UPtGe. This is connected with a closer packing of conduction-electron states with respect to energy in the gapped state, which increases the value of the derivative $\partial N_f/\partial E$ and hence determines its strongly peaked temperature dependence.

The characteristic features due to the band-gap opening at $E_F$ below the Néel temperature ($T_N = 17.5$ K) have also been reported in single-crystalline measurements of tetragonal $URu_2Si_2$.[30] However, in this case the negative sharp maxima of the TEP appear at about 13 K reaching magnitudes of $-25$ and $-48\ \mu$V/K for $S_a$ and $S_c$, respectively. In $URu_2Si_2$, a change in the sign of $S(T)$ at $T \simeq 70$ K, i.e., well above the ordering temperature, has been attributed to competing contributions due to multibands with a hole character and with an electron character, respectively.

Finally, we want to mention that an analogue situation in the behavior of $S(T)$ was also reported in the detailed work of Paschen *et al.*[31] for single-crystalline CeNiSn, having characteristic features of the opening of a pseudogap in the DOS at $E_F$, which drives the $S_i(T)$ through pronounced maxima at low temperatures. However, the reasons of a pseudogap arising in CeNiSn are not connected with the onset of a magnetic ordered state. The above discussion clearly indicates that the sharp maxima at low temperatures in $S(T)$ of a number of Ce and U intermetallics have different origins. Further detailed studies on this subject are needed in order to formulate a quantitative description of $S(T)$ in strongly correlated electron systems.

## IV. CONCLUSIONS

The results of measurements of the temperature and magnetic field dependences of the magnetic susceptibility, electrical resistivity, and thermoelectric power point toward a strong out-of-plane anisotropy in the electronic behavior of UPtGe. The reason for the existence of the anisotropy is associated with the rare crystal structure of UPtGe,[10] and with the formation of an incommensurate cycloid of magnetic moments that are confined to the $ac$ plane and propagating along the $a$ direction.

Despite the large difference in the $a$ and $c$ lattice parameters (see Table I) the $\chi_a$ and $\chi_c$ susceptibilities were found to be nearly identical, due to a magnetically near-isotropic situation in this case. The coupling between magnetic moments residing in successive $ac$-planes is much weaker than the in-plane coupling, on account of the much larger $|\theta_P|$ value that we observe for the susceptibility along the $b$ direction. A recent preliminary optical spectroscopic study performed on single-crystal UPtGe (Ref. 32) inferred a much stronger localization along the $b$ axis than those along the other two directions. The $b$ direction was also found in the present study to be the only direction that yields saturation of the resistivity $\rho(T)$ towards the ground state, together with a positive metalliclike magnetoresistivity at low temperatures. We explained the observed large differences in $\rho_i(T)$ and in the isothermal MR between the moment-plane measurements ($i \| a,c$) and the out-of-plane data ($i \| b$) in terms of the periodicity of the ordered-moment alignment. The thermoelectric power and in particular the sharp peaking behavior for UPtGe was put into perspective with that of two other strongly anisotropic magnets, viz. UNiAl and $URu_2Si_2$, and with that of the nonordered Kondo semiconductor CeNiSn.

UPtGe is a special example of a $5f$-electron system displaying anomalous behavior in its physical properties. It has a crystallographic and magnetic structure that is indeed unique among the actinide family of intermetallic compounds. Further theoretical studies as well as experimental measurements are desired in order to investigate the complex physics at work in this compound, in relation to other equiatomic ternary uranium derivatives as well as in relation to the broader class of strongly correlated electron systems.

## ACKNOWLEDGMENTS

We gratefully acknowledge the help of Professor Takemi Komatsubara in growing of the single crystals. This research is based upon work supported by the State Committee for Scientific Research (KBN) within Grant No. 2PO3B 109 24, and the South African National Research Foundation (Grant No. 2049198). It is a pleasure to thank Mr. Roman Gorzelniak (M.Sc) and Mr. Dariusz Badurski (M.Sc) for expert technical assistance in performing the measurements reported in this work. We thank Professor V. Niezhankovski for performing the Hall coefficient measurements in the International Laboratory of Low Temperature and High Fields in Wrocław.

*Email address: ams@na.rau.ac.za

[1] V. Sechovsky and L. Havela, in *Handbook of Magnetic Materials*, edited by K.H.J. Buschow (Elsevier, Amsterdam, 1998), Vol. 11.
[2] R. Troć and V.H. Tran, J. Magn. Magn. Mater. **73**, 389 (1988).
[3] V.H. Tran, R. Troć, and D. Badurski, J. Magn. Magn. Mater. **87**, 291 (1990).
[4] L. Havela, A. Kolomiets, V. Sechovsky, M. Diviš, M. Richter, and A.V. Andreev, J. Magn. Magn. Mater. **177-181**, 47 (1988).
[5] S. Kawamata, K. Ishimoto, H. Iwasaki, N. Kobayashi, Y. Tamaguchi, T. Komatsubara, G. Kido, T. Mitsugashira, and Y. Muto, J. Magn. Magn. Mater. **90&91**, 513 (1990).
[6] S. Kawamata, H. Iwasaki, N. Kobayashi, K. Ishimoto, Y. Yamaguchi, and T. Komatsubara, J. Magn. Magn. Mater. **104-107**, 53 (1992).

[7] A. Szytuła, M. Kolenda, R. Troć, V.H. Tran, M. Bonet, and J. Rossat-Mignod, Solid State Commun. **81**, 481 (1992).
[8] R.A. Robinson, A.C. Lawson, J.W. Lynn, and K.H.J. Buschow, Phys. Rev. B **47**, 6138 (1993).
[9] S. Kawamata, K. Ishimoto, Y. Yamaguchi, and T. Komatsubara, J. Magn. Magn. Mater. **104-107**, 51 (1992).
[10] D. Mannix, S. Coad, G.H. Lander, J. Rebizant, P.J. Brown, J.A. Paix̃ao, S. Langridge, S. Kawamata, and Y. Yamaguchi, Phys. Rev. B **62**, 3801 (2000).
[11] R. Troć and A.M. Strydom, J. Magn. Magn. Mater. (to be published).
[12] G.M. Sheldrick, SHELX-97, Program for Crystal Structure Refinement, University of Göttingen, Germany, 1997.
[13] R.-D. Hoffmann, R. Pöttgen, G.H. Lander, and J. Rebizant, Solid State Sci. **3**, 697 (2001).
[14] R. Troć, V.H. Tran, M. Kolenda, R. Kruk, K. Łatka, A. Szytuła, J. Rossat-Mignod, M. Bonnet, and B. Buchner, J. Magn. Magn. Mater. **151**, 102 (1995).
[15] L.M. Sandratskii and G.H. Lander, Phys. Rev. B **63**, 134436 (2001).
[16] S. Kawamata, H. Iwasaki, and N. Kobayashi, J. Magn. Magn. Mater. **104-107**, 55 (1992).
[17] S. Kawamata, G. Kido, K. Ishimoto, Y. Yamaguchi, H. Iwasaki, N. Kobayashi, and T. Komatsubara, Physica B **177**, 169 (1992).
[18] K.H.J. Buschow, E. Brück, R.G. van Wierst, F.R. de Boer, L. Havela, V. Sechovsky, P. Nozar, E. Sugiura, M. Ono, M. Date, and A. Yamagashi, J. Appl. Phys. **67**, 5215 (1990).
[19] F.R. de Boer, K. Prokeš, H. Nakotte, E. Brück, H. Hilbers, P. Svoboda, V. Sechovsky, L. Havela, and H. Mallets, Physica B **201**, 251 (1994).
[20] See for example, T. Takabatake, T. Sasakawa, J. Kitagawa, T. Suemitsu, Y. Echizen, K. Umeo, M. Sera, and Y. Bando, Physica B **328**, 53 (2003).
[21] A. Grauel, D. Fromm, C. Geibel, F. Steglich, N. Sato, and T. Komatsubara, Int. J. Mod. Phys. B **7**, 50 (1993).
[22] D. Jaccard and J. Sierro, in *Valence Instabilities*, edited by P. Wachter and H. Boppart (North-Holland, Amsterdam, 1982), p. 409.
[23] K.H. Fischer, Z. Phys. B: Condens. Matter **76**, 315 (1999).
[24] Y. Yamaguchi, J. Sakurai, F. Tereshina, H. Kawanaka, T. Takabataka, and H. Fuyii, J. Phys.: Condens. Matter **2**, 5715 (1990).
[25] N.F. Mott and H. Jones, in *The Theory of the Properties Metals and Alloys* (Oxford University Press, New York, 1958).
[26] Y. Bando, T. Suemitsu, K. Takagi, H. Tokushima, Y. Echizen, K. Katoh, K. Umeo, Y. Maeda, and T. Takabatake, J. Alloys Compd. **313**, 1 (2000).
[27] K. Prokeš, S. Fukuda, and J. Sakurai, Physica B **270**, 221 (1999).
[28] K. Prokeš, F. Bourdarot, P. Burlet, P. Javorsky, M. Olšovec, V. Sechovsky, E. Brück, F.R. de Boer, and A.A. Menovsky, Phys. Rev. B **58**, 2692 (1998).
[29] F.J. Blatt, P.A. Schroeder, C.L. Foiles, and D. Greig, in *Thermoelectric Power of Metals* (Plenum Press, New York, 1976).
[30] J. Sakurai, K. Hategawa, A.A. Menovsky, and J. Schweizer, Solid State Commun. **97**, 689 (1996).
[31] S. Paschen, B. Wand, G. Sparn, F. Steglich, Y. Echizen, and T. Takabatake, Phys. Rev. B **62**, 14 912 (2000).
[32] J. Schoenes, U. Barkow, M. Marutzky, H. Schroter, R. Troć, and T. Komatsubara (unpublished).